Spectroscopic Implications of Partially Quenched Orbital Angular Momentum in the OH−Water Complex†

Mark D. Marshall‡

Department of Chemistry, Amherst College, P.O. Box 5000, Amherst, Massachusetts 01002-5000

Marsha I. Lester*

Department of Chemistry, University of Pennsylvania, Philadelphia, Pennsylvania 19104-6323

Received: August 16, 2004; In Final Form: November 8, 2004

The OH monomer orbital angular momentum is predicted to be partially quenched in the OH−water complex because of the significant splitting of the OH monomer orbital degeneracy into $^2A'$ and $^2A''$ electronic states. This orbital angular momentum quenching and the associated decoupling of the electron spin from the *a* inertial axis are shown to have dramatic effects on the rotational band structure of the microwave and infrared transitions of the OH−water complex. At the ab initio values for the splitting between the $^2A'$ and $^2A''$ surfaces, simulated spectra of a- and b-type bands, such as those expected for the OH radical stretch and water asymmetric stretch, are predicted to have a noticeably different appearance than the well-established limiting cases associated with fully quenched or completely unquenched orbital angular momentum. Spectral identification of the OH−water complex in the gas phase will require explicit consideration of this quenching phenomenon.

I. Introduction

Hydroxyl radicals are expected to form strong hydrogen bonds with water, and thus, complexes of the OH radical with water may be important in a variety of environments. These include the gaseous environment of the atmosphere,[1,2] the heterogeneous interface of liquid water droplets and/or ice crystals,[3,4] and the bulk regions of liquid water, snow, and ice, particularly upon radiolysis or photolysis.[5−7] Spectroscopic studies of binary OH−water complexes are expected to shed new light on the intermolecular interaction between the OH radical and the water molecule in these environments. This paper shows that the rotational band structure of microwave and infrared transitions of the OH−water complex, typically used for spectral identification, may be quite complicated and very different from analogous closed-shell systems due to partial quenching of the OH monomer's orbital angular momentum in the complex.

Extensive ab initio calculations have shown that the global minimum on the OH + H_2O potential energy surface is a C_s structure, H_2O−HO, in which hydrogen bonding occurs between the H atom of the hydroxyl radical (donor) and the O atom in the water molecule (acceptor)[8,9] as shown in Figure 1. The energy of the planar structure (Figure 1) is calculated to be less than 40 cm^{-1} higher,[9] and the two equivalent structures, with the water tilted "up" and "down", are expected to be connected by large amplitude vibrational zero-point motion through this small barrier, as is the case for the analogous closed-shell species, water−HF.[10] Early calculations had suggested that the OH radical functioned as a hydrogen bond acceptor,[11] but this configuration has since been shown to be a local minimum on the potential and not the global minimum. The hydrogen bond distance is predicted to be ∼1.95 Å at the global minimum, which is analogous to the water dimer, although the computed well depth of ∼5.7 kcal mol^{-1} for OH−water is somewhat greater than that for the water dimer (4.9 kcal mol^{-1}).[12] The water dimer has been predicted and recently shown to be present at significant concentrations in the atmosphere,[12−15] and the even larger binding energy of the OH−water complex suggests that a portion of the OH radicals in the atmosphere may be present in this form.

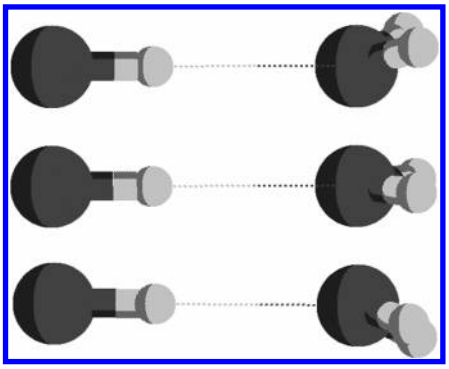

Figure 1. Two equivalent structures at the global minimum of the OH + H_2O potential energy surface, with water tilted up (top) and down (bottom), and the planar transition state (middle) that connects the equilibrium configurations, adapted from the ab initio calculations of ref 9. Vibrational zero-point motion is expected to average over these configurations, leading to an effective planar geometry for the OH−water complex.

As shown for other OH-containing complexes,[16,17] there are two relevant potentials of $^2A''$ and $^2A'$ symmetry, differing only by the orientation of the half-filled pπ orbital of OH with respect to the nuclear framework, which are derived from the interaction of an OH $X\ ^2\Pi$ radical with a water molecule. The symmetry plane in OH−water passes through the heavy atoms and bisects the HOH angle of the water molecule. The $^2A'$ and $^2A''$ potential

† Part of the special issue "George W. Flynn Festschrift".

* To whom correspondence should be addressed. E-mail: milester@sas.upenn.edu.

‡ On sabbatical leave at the University of Pennsylvania during 2003−04.

10.1021/jp046308k CCC: $30.25
Published on Web 02/05/2005

surfaces correspond to the half-filled pπ orbital of the OH radical lying within and perpendicular to this symmetry plane, respectively.[18] Nuclear motion is expected to sample both of these electronic surfaces, since they lie close to one another in the vicinity of the global minimum.[9]

There are several reports in the literature of the OH−water complex being detected in ice films and argon matrices. Three recent studies report infrared spectroscopic transitions attributed to the OH−water complex,[19−21] although it may also have been detected in earlier studies. The complex has been produced through an rf discharge of a gaseous H_2O−Ar mixture prior to deposition on a cold window[19,21] and by UV photolysis at 266 nm of a mixture of HO_2 and H_2/D_2 already embedded in an argon matrix.[20] Features observed near 3452.2 and 3428.0 cm^{-1} are attributed to the OH radical stretch for the OH−water complex in different sites of the Ar matrix;[19,21] these are shifted about −100 cm^{-1} from uncomplexed OH in the matrix. Features have also been reported in the asymmetric stretching region of H_2O near 3727.6 cm^{-1},[20] with multiple peaks again arising from different matrix sites or possibly hindered rotational motion but with little shift from the associated H_2O−ν_3 transition. The matrix studies and complementary theory provide good estimates for the vibrational frequencies of the OH−water complex in the gas phase.

In preparation for planned experiments on the OH−water complex in the gas phase, we wanted to predict the rotational band structure associated with microwave and infrared transitions of the complex. While previous studies can be used to estimate the vibrational frequencies of the OH−water complex, there has been no previous consideration of the rotational band structure associated with these transitions in this open-shell complex. The rotational band structure is expected to be strongly affected by the coupling between the spin and/or orbital angular momenta of the OH radical with the overall rotation of the complex. Furthermore, partial quenching of these OH angular momenta upon complexation can dramatically change the appearance of the rotational band contour, as demonstrated previously in the theoretical modeling and experimental spectra of the OH−acetylene complex.[16,22,23] Such quenching is induced when the difference potential, ρ, the energy difference between the $^2A''$ and $^2A'$ surfaces in nonlinear configurations, is comparable in magnitude to the spin−orbit coupling constant for the OH monomer ($\alpha = -139$ cm^{-1}). Various ab initio calculations predict a difference potential of approximately −110 cm^{-1} (the negative sign indicates the $^2A'$ state is of lower energy) and −190 cm^{-1} for OH−water at its equilibrium geometry,[9,21,24] indicating that gas-phase OH−water spectra could exhibit a very complicated rotational band structure arising from the partial quenching of the OH orbital angular momentum in the complex. This paper presents model calculations that reveal the evolution of the rotational energy levels for the interacting pair of molecules between the limits of completely unquenched and fully quenched OH orbital angular momentum in the complex. It also illustrates how these changes in the rotational energy levels are expected to be manifested in the microwave and infrared spectra of the OH−water complex.

II. Theoretical Methods

Marshall and Lester have developed a model to treat the rotational energy level structure of OH-containing complexes with arbitrary quenching of the electronic orbital angular momentum and to predict their infrared spectra.[22] In addition to terms representing the rotational motion of the complex and the spin−orbit interaction of the OH monomer, the Hamiltonian contains the operator

$$\hat{H}_q = \frac{\rho}{2}(\bar{l}_+^{\,2} + \bar{l}_-^{\,2}) \qquad (1)$$

which causes the splitting of the OH monomer orbital degeneracy into $^2A'$ and $^2A''$ electronic states that is responsible for the quenching. In eq 1, ρ is the difference potential, averaged over the vibrational motion of the complex, and the bars over the electronic orbital raising and lowering operators indicate that they are "normalized" by the effective value of $l(l+1)$ for the molecule.

Rotational wave functions were constructed using a primitive set of basis functions

$$|JpM\lambda\sigma\rangle = |JpM\rangle|\eta\lambda\rangle|s\sigma\rangle \qquad (2)$$

where J is the total angular momentum excluding nuclear spin, p is its projection onto the a inertial axis of the complex, and M is its projection onto a space-fixed axis. The projections of orbital and spin angular momenta, $l = 1$ and $s = {}^1/_2$, of the unpaired electron onto the OH axis are given by $\lambda = \pm 1$ and $\sigma = \pm {}^1/_2$, respectively, and their sum is designated $\omega = \lambda + \sigma$. The quantum number η is included to allow for the general case of different electronic states with the same value of λ. Linear combinations of these primitive functions produce wave functions of definite parity

$$|JP\lambda\sigma\epsilon\rangle = (1/2)^{1/2}[|J,P,\lambda,\sigma\rangle + \epsilon(-1)^{J-(1/2)}|J,-P,-\lambda,-\sigma\rangle] \qquad (3)$$

where $P \equiv |p|$, $\epsilon = \pm 1$, and M is suppressed in the absence of an external field. Rotational energy levels are calculated via diagonalization of the complete Hamiltonian matrix that results within the framework of the two interacting electronic states, $^2A'$ and $^2A''$.

Although the equilibrium configuration of the OH−water complex has C_s symmetry, the barrier to planarity in the complex is predicted to be quite small (<40 cm^{-1}).[9] This is considerably smaller than the barrier found for the related closed-shell species water−HF (126 cm^{-1}),[10] where zero-point motion results in an effectively planar geometry for the complex. A similar situation will certainly occur in OH−water, and consequently, the rovibrational states of this molecule will possess C_{2v} symmetry so that the model,[22] originally developed for the T-shaped OH−acetylene complex, may be applied directly. As a further consequence of this large amplitude motion, OH−water will have ortho and para spin modifications that will not interconvert under most experimental conditions.

TABLE 1: Parameters (in cm^{-1}, except as noted) Used To Simulate Spectra for OH−Water

parameter	value	parameter	value
A	13.13[a]	ν_{asym}	3749
$(B+C)/2$	0.22	Γ_{OH}	0.15
$(B-C)/2$	0.0015	Γ_{asym}	0.03
α	−139	T_{rot}	5 K
ν_{OH}	3471		

[a] The value is reduced to 13.03 cm^{-1} for the $v = 1$ state of the water asymmetric stretch.

The spectroscopic constants (Table 1), used to model the rotational energy levels for OH−water, are estimated using a combination of ab initio predictions and analogies to the related water−HF[10,25−27] and water−HCl[28] complexes. The B and C rotational constants are primarily determined by the monomer

geometries, assumed to be unchanged,[29,30] and the hydrogen bond length, taken as 1.95 Å from ab initio results.[9] The value for the *A* rotational constant of the complex, however, while approximately equal to the *B* constant of water, is a sensitive function of vibrational averaging over the H_2O out-of-plane motion. We have chosen a value of 13.13 cm^{-1}, appropriate for a 25° average out of plane angle, by comparison to the HF and HCl complexes. Several values of ρ are used to demonstrate the effect of the difference potential on the form of the spectrum for the complex. Ab initio results indicate values of −110 and −190 cm^{-1} for ρ,[9,21,24,31] and in addition to these, simulations of spectra with $\rho = 0$ and −5000 cm^{-1} are used to illustrate the limits of very small and very large difference potentials, respectively. The spin−orbit constant for the OH radical is assumed to remain unchanged upon complexation.

The OH radical stretching band and the water asymmetric stretching band are both predicted to have significant intensity.[9,21,31] The intensity for the OH radical stretch is dramatically increased from the monomer value, while the water-based vibrational band intensities are all similar to the isolated H_2O molecule. Spectra for these two bands are simulated from the calculated rotational energy levels by assuming that the directions of the transition moments are unchanged from those of the monomer. This leads to an a-type band for the OH radical stretch and a b-type band for the water asymmetric stretch, and previously given expressions for transition moment matrix elements are used.[22] Ab initio results for frequency shifts from monomer values[9] are used to estimate values for the respective band origins, ν_{OH} and ν_{asym}. Line widths, Γ_{OH} and Γ_{asym}, observed for the analogous bands in the infrared spectrum of the water dimer,[32] as reassigned by Huisken et al.,[33] are used in the simulations (see Table 1), and a rotational temperature appropriate for a supersonic expansion, $T_{rot} = 5$ K, is assumed. As was observed for OH−acetylene,[16,23] all spectroscopic constants are assumed to remain unchanged upon vibrational excitation with the exception of the *A* rotational constant for the water asymmetric stretching band. In this case the constant is reduced by the same factor, 0.9924, observed for excitation of the corresponding band in the water monomer.[34,35] Pure rotational transition frequencies for the ground vibrational state are also determined from the model.

III. Results

The rotational energy levels of the OH−water complex group into manifolds according to the value for the projection of an angular momentum along the *a* inertial axis of the complex in both limiting cases, that of negligible energy difference between the $^2A'$ and $^2A''$ states as well as that of well-separated states. Figure 2 shows the energies of the first few rotational levels in each manifold, referenced to a common energy origin, as a function of the ratio of the difference potential to the monomer spin−orbit coupling constant, α. The logarithmic scale, $\ln \sqrt{(\rho/\alpha^2+1)}$, chosen for the abscissa of the figure reflects the strength of the coupling responsible for the quenching of orbital angular momentum. It also allows for easy visualization of the strong dependence of the energies on the difference potential for small values of the ratio while compressing the weaker dependence at larger ratios.

On the left side of Figure 2 with $\rho = 0$, the manifolds are characterized by the half-integer projection, *P*, of the total angular momentum, *J*, with contributions from molecular rotation, electronic orbital, and electronic spin angular momentum. Likewise, the energy differences between rotational levels on the left side of the diagram are *odd* multiples of $(B + C)/2$,

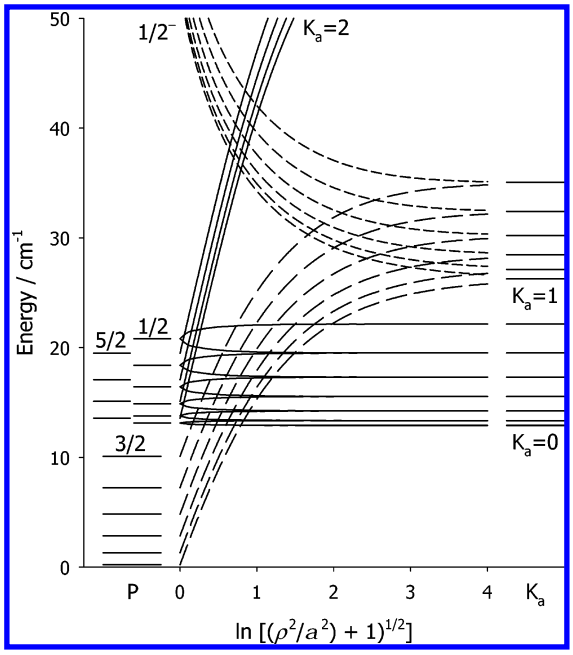

Figure 2. Correlation diagram showing the energies (minus $\sqrt{\rho^2+\alpha^2}/2$) of the rotational manifolds for OH−water as a function of the ratio of the difference potential, ρ, to the monomer spin−orbit coupling constant, α. The first few rotational levels of each manifold on the left are labeled with the value of the half-integer projection quantum number, *P*, and a superscript indicating if ω is negative. The value of $|P - \omega|$ is indicated by the line style: 0 for dashed, 1 for solid, and 2 for short-dashed. As the difference potential increases, the electronic orbital angular momentum is quenched, and the manifolds evolve into the limiting case on the right in which rotational levels are characterized by the integer projection quantum number, K_a. For example, the $P = 1/2$, $\omega = +3/2$ levels evolve to $K_a = 0$, while the $P = 5/2$, $\omega = +3/2$ levels evolve to $K_a = 2$.

as expected for strong coupling of the electronic spin to the molecular axes. For each level shown in this lower of the two spin−orbit components, the projections of the electronic orbital and spin angular momenta sum to give $|\lambda + \sigma| = |\omega| = 3/2$. The lowest-energy manifold has $P,\omega = 3/2, +3/2$, while the higher-energy $P,\omega = 5/2, +3/2$ and $P,\omega = 1/2, +3/2$ manifolds are nearly degenerate in this limit. Furthermore, due to the large *A* rotational constant expected for OH−water, only the lowest manifolds of each spin modification, namely, those with $|P - \omega| = 0, 1$, will have a significant population at the low rotational temperatures of a supersonic expansion.

As the difference potential increases, the electronic orbital angular momentum is quenched and with it the magnetic field responsible for coupling the electron spin to the *a* inertial axis. Levels with $P,\omega = 1/2, -3/2$ descend in energy to become one spin component of the $K_a = 1$ manifold, while those with $P,\omega = 3/2, +3/2$ increase in energy to become the other spin component. Similarly, levels with $P,\omega = 5/2, +3/2$ rapidly increase in energy and correlate to $K_a = 2$ levels. The $P,\omega = 1/2, +3/2$ levels show the effects of parity splitting as they evolve into $K_a = 0$ levels. Eventually, when the difference potential is much larger than the spin−orbit splitting, the electronic orbital angular momentum is fully quenched, and the limit on the right side of Figure 2 is reached. Now, the appropriate angular momentum, *N*, is an integer as it excludes electron spin, and the manifolds are labeled with K_a, the projection of *N*. Rotational energy level spacings are *even* multiples of $(B + C)/2$ on the right side of the diagram, as appropriate for an integer rotational quantum number. Once

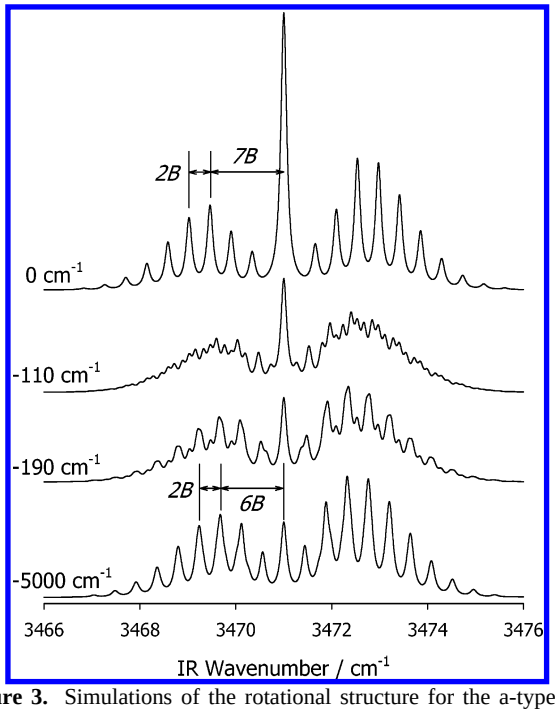

Figure 3. Simulations of the rotational structure for the a-type OH radical stretching band of the OH−water complex at four values of the difference potential, ρ. In the limiting cases of $\rho = 0$ and 5000 cm^{-1}, the spectrum shows the PQR branch contour of a near symmetric top, but with P and R branch features switching from *odd* to *even* multiples of $(B + C)/2$ with respect to the central Q branch. At the intermediate values of ρ expected for OH−water, the structure of the P and R branches is more complicated.

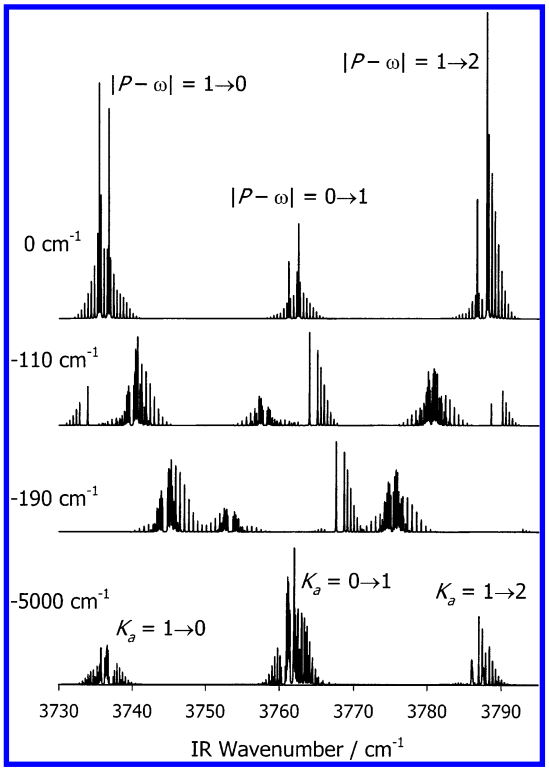

Figure 4. Simulations of the rotational structure for the b-type water asymmetric stretching band of the OH−water complex at four values of the difference potential, ρ. The appearance of the spectrum is very sensitive to the value of ρ and, for very large values of ρ/α, becomes identical to that of a chemically bound radical in a doublet electronic state with $\Delta K_a = \pm 1$ sub-bands. In the limit of small ρ, the sub-bands are attributed to ± 1 changes in $|P - \omega|$.

again, only the lowest manifold for each spin modification, $K_a = 0, 1$, will be populated at the low temperatures of a supersonic expansion.

Figure 3 shows the simulated OH stretching fundamental band for OH−water at four different values of the difference potential. For both limiting cases, the small difference potential with $\rho = 0$ cm^{-1} at the top and the large difference potential with $\rho = -5000$ cm^{-1} at the bottom, the band has the simple PQR branch contour expected for a parallel (a-type) band in this very near prolate asymmetric top. It is unlikely that any sub-band structure will be resolved for this band in the OH−water spectrum, since the analogous band in $(H_2O)_2$ has a 0.15 cm^{-1} line width[32,33] because of vibrational predissociation. A similar line width in OH−water would result in individual rotational lines merging into inhomogeneously broadened features spaced by twice the effective rotational constant, $(B + C)/2$. There is, however, a clear difference between the two limiting cases of small and large difference potentials: the P and R branch features are displaced from the central Q branch by *odd* multiples of this constant for $\rho = 0$ cm^{-1} and by *even* multiples for $\rho = -5000$ cm^{-1}. The Q branch in the $\rho = 0$ cm^{-1} spectrum has greater relative intensity because all of the populated rotational levels have allowed $\Delta J = 0$ transitions in this limit, but $\Delta N = 0$ transitions are only allowed for $K_a > 0$ in the large difference potential limit.

For intermediate values of the difference potential, the band structure becomes more complicated as each manifold evolves at a different rate between the two limits. This can be seen in Figure 2 where, for example, the $P,\omega = 1/2, +3/2$ levels approach the limiting $K_a = 0$ behavior at much smaller values of the difference potential than those with $P,\omega = 3/2, +3/2$ approach their $K_a = 1$ limiting behavior. Consequently, the P and R branch features are split by sub-band structure that would be apparent even at the expected predissociation line width of 0.15 cm^{-1}. This can be seen in the spectra for $\rho = -110$ and -190 cm^{-1} in Figure 3. This behavior is somewhat different from that predicted for OH−acetylene.[22] In that complex with a much smaller *A* rotational constant (1.217 cm^{-1}), many more rotational manifolds are populated causing the sub-band structure to be washed out and resulting in an inhomogeneous broadening of the features.

Figure 4 shows the simulated water asymmetric stretching fundamental band for the same four values of the difference potential. Since this perpendicular band follows b-type selection rules, the projection quantum number changes in the transition from the ground to excited vibrational state. Consequently, the transition frequencies and, in turn, the band contour will be more sensitive functions of the difference potential than for the OH stretching fundamental. In both limiting cases, the band has the expected structure for a perpendicular transition of a nearly prolate symmetric top with well-spaced sub-bands separated by approximately 2*A*. The branches in each sub-band, most notably the Q branches, are doubled. For small values of the difference potential, as in the spectrum at the top of the figure, the doubling is attributed to the Coriolis splitting that, for example, causes the rotational levels with $(P - \omega) = \pm 1$ to have slightly different energies. For the limiting case at the bottom, with a large difference potential, the doubling is the familiar spin splitting of chemically bound radicals in doublet electronic states. The effect of nuclear spin statistics can be seen in the different relative intensities of the central and outer sub-bands in the two limits as the relative ordering of the manifolds with ortho and para nuclear spins switches from small ρ to large ρ.

In the simulated bands for $\rho = -110$ and -190 cm^{-1} in the center of Figure 4, the central $|P - \omega| = 0 \rightarrow 1$ sub-band of

TABLE 2: Selected Microwave Rotational Transition Frequencies[a] (in GHz) for OH−Water

J''	J'	P^b	ϵ''	N''	N'	K	$\rho = 0$ cm^{-1}	$\rho = -110$ cm^{-1}	$\rho = -190$ cm^{-1}	$\rho = -5000$ cm^{-1}
1/2	1/2	$1/2^+$	+1	0	1	0	−[c]	8.18	10.65	13.18
1/2	3/2	$1/2^+$	+1	0	1	0	19.76	15.68	14.46	13.19
3/2	3/2	$1/2^+$	−1	1	2	0	−[c]	16.37	21.29	26.37
1/2	3/2	$1/2^+$	−1	1	2	0	19.76	23.86	25.10	26.38
3/2	5/2	$1/2^+$	−1	1	2	0	32.93	28.86	27.64	26.38
3/2	5/2	$3/2^+$	+1	1	2	1	32.93	32.88	32.81	29.55
3/2	5/2	$3/2^+$	−1	1	2	1	32.93	32.88	32.82	29.69
5/2	5/2	$1/2^+$	+1	2	3	0	−[c]	24.56	31.94	39.56
3/2	5/2	$1/2^+$	+1	2	3	0	32.93	37.04	38.29	39.57
1/2	3/2	$1/2^-$	+1	1	2	1	−[d]	−[d]	−[d]	21.92
1/2	3/2	$1/2^-$	−1	1	2	1	−[d]	−[d]	−[d]	22.06

[a] The selection rules for quantum numbers not explicitly listed for both levels are $\Delta P = 0$, $\Delta K = 0$, $\Delta\omega = 0$, and $\epsilon = \pm 1 \rightarrow \mp 1$. [b] All levels have $|\omega| = 3/2$; the sign of ω is indicated by a superscript on P. [c] The two levels in this Q branch transition are degenerate for $\rho = 0$ and parity split when $|\rho| > 0$. [d] The transition has negligible intensity in the jet-cooled spectrum until the initial level becomes populated for large values of $|\rho|$.

the small ρ limit is seen to split into two features that move outward and eventually become the $K_a = 1 \rightarrow 0$ and $K_a = 1 \rightarrow 2$ sub-bands of the large ρ limit. At the same time portions of the outer two sub-bands for $\rho = 0$ cm^{-1}, $|P - \omega| = 1 \rightarrow 0$, $1 \rightarrow 2$, move inward with increasing difference potential as they combine into the $K_a = 0 \rightarrow 1$ sub-band at the bottom of the figure.

The pure rotational spectrum of OH−water will follow a-type selection rules and, in principle, resemble the R branch of the OH stretching fundamental infrared transition. Of course, the line width for this spectrum will be much narrower, as the upper state is not predissociative, and the effects of interactions such as centrifugal distortion, λ-doubling, and magnetic hyperfine interactions, which are ignored in the present model, will play a role in determining actual transition frequencies. Preliminary calculations indicate that the largest of these effects will be on the order of a few to several tens of megahertz.[36] Nevertheless, the current model is adequate for understanding the qualitative features of the OH−water spectrum at microwave frequencies. Table 2 contains frequency predictions, and Figure 5 shows the resulting stick spectra from 5 to 30 GHz for the complex at four values of the difference potential.

For $\rho = 0$ cm^{-1}, the rotational spectrum consists of equally spaced lines whose frequencies, ignoring the extremely small asymmetry splitting, are given by $\nu = 2(J'' + 1)(B + C)/2$. Because J is a half-integer, the lines are at *odd* multiples of $(B + C)/2$, with the first transition, $J = 1/2 \rightarrow 3/2$, $P = 1/2$, $\omega = +3/2$, appearing at $3(B + C)/2$. Given the estimated values of the rotational constants for OH−water, the transition at 19.76 GHz would be the only one in the 5−30 GHz interval. Indeed, for moderate values of the difference potential, the centimeter wave spectrum has lines exclusively from levels in the P, $\omega = 1/2$, $+3/2$ manifold. These levels show the effects of parity splitting[22,37] as ρ increases, as shown in the correlation diagram of Figure 2. The effect on the rotational spectrum is seen in Figure 5 for $\rho = -110$ cm^{-1} where the $J = 1/2 \rightarrow 3/2$ line, $^qR(1/2)$, has split into two parity components at 15.68 and 23.86 GHz, while the lower-frequency component of the $J = 3/2 \rightarrow 5/2$ transition, $^qR(3/2)$ at 28.86 GHz, has moved into this frequency region. In the limit of small ρ, the lines are labeled using a straightforward extension of symmetric top branch notation, $^{\Delta P}\Delta J(J'')$. In addition to these R branch transitions, Q branch transitions across the parity doublets can be seen at 8.18, 16.37, and 24.56 GHz for $J = 1/2$, 3/2, and 5/2, respectively. The parity splitting increases with ρ as comparison with the spectrum for $\rho = -190$ cm^{-1} demonstrates.

In the limit of very large difference potential, as shown in Figure 5 with $\rho = -5000$ cm^{-1}, the orbital angular momentum is completely quenched and the parity splitting reaches its maximum value of $B + C$. The rotational transitions are now centered at *even* multiples of $(B + C)/2$, indicating that the rotational motion is characterized by the integer quantum number N, and the lines labeled by $^{\Delta K_a}\Delta N(N'')$. The strong lines in the spectrum for $\rho = -5000$ cm^{-1} at 13.18 and 26.38 GHz are the $N = 0 \rightarrow 1$ and $1 \rightarrow 2$ transitions, $^qR(0)$ and $^qR(1)$, for $K_a = 0$.[38] In the limit of large ρ, $^qQ(1/2)$ and the lower frequency component of $^qR(1/2)$ merge into the two spin components of $^qR(0)$, while $^qQ(3/2)$, the upper frequency component of $^qR(1/2)$, and the lower frequency component of $^qR(3/2)$ combine to become a spin-split $^qR(1)$ line. The pairs of doublets centered at 21.99 and 29.62 GHz are the two spin components of the $N = 1 \rightarrow 2$ transition for $K_a = 1$. The smaller splitting within each pair is the familiar asymmetry splitting for this value of K_a in asymmetric tops.

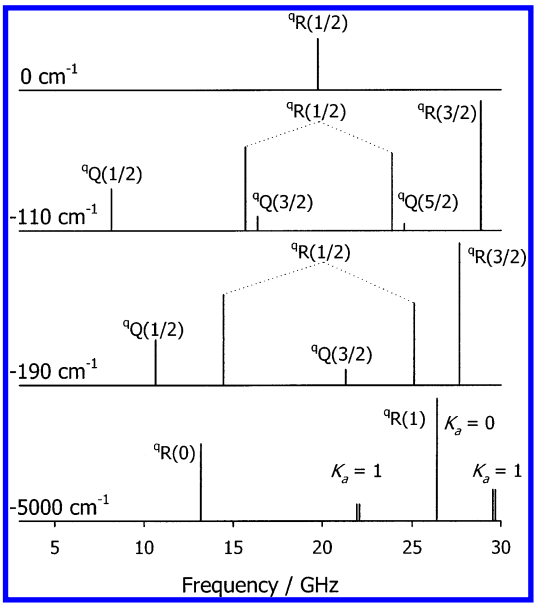

Figure 5. Simulations of the pure rotational spectrum for the OH−water complex in the 5−30 GHz region as a function of the difference potential, ρ. The spectral lines arise primarily from levels in the $P = 1/2$, $\omega = +3/2$ manifold and, thus, exhibit parity splitting with increasing ρ, as illustrated in the evolution of $^qR(1/2)$ into $^qR(0)$ and $^qR(1)$ lines with $K_a = 0$. Lines are labeled using the notation $^{\Delta P}\Delta J(J'')$ and $^{\Delta K_a}\Delta N(N'')$ in the low and high ρ limits, respectively. The rotational transitions shift from *odd* to *even* multiples of $(B + C)/2$ in evolving from the low to high ρ limits.

IV. Discussion

The spectra, predicted in the previous section, demonstrate that the influence of partially quenched electronic orbital angular

momentum on the rotational energy levels of the OH−water complex will have profound implications on its infrared and microwave spectra. In particular, the rotational band structure will be very different from the structurally similar water dimer molecule, since the spectra for the entire range of values for the difference potential predicted by ab initio theory will be far from the large ρ limit appropriate for the closed-shell $(H_2O)_2$ species. With only two equivalent frameworks that interconvert in an extremely facile manner, OH−water spectra will not show the complications of interconversion tunneling between multiple minima (8 for water dimer). Furthermore, the particular shapes of the infrared band contours and values of the microwave transition frequencies are quite sensitive to the precise value of the difference potential within its predicted range.

For the OH radical stretching band, the homogeneous line width from the vibrational predissociation of the individual transitions may reduce its sensitivity to ρ. The vibrational motion excited in this band is directly coupled to the dissociation coordinate, which could contribute to a short lifetime. The analogous fundamental in $(H_2O)_2$, which is slightly less strongly bound than is OH−water, had $\sim$0.14 cm^{-1} line widths,[32,33] presumably as a consequence of rapid vibrational predissociation. Nevertheless, the spectra simulated in Figure 3 using a 0.15 cm^{-1} Lorentzian line width demonstrate that a clear dependence on ρ may be expected in this a-type band contour even for lines this broad.

OH stretching motions based on the water portion of OH−water are not directly coupled to complex dissociation, and absent an efficient resonant channel, vibrational predissociation should be much slower for these vibrations. Indeed, for $(H_2O)_2$, line widths for the acceptor asymmetric OH stretching fundamental band were observed to range from 0.0017 to 0.03 cm^{-1}, displaying a dependence on both K and tunneling level.[32] Even at the largest line width in this range, used to simulate the spectra in Figure 4, individual lines in the P and R branches are well-resolved. In addition to more detailed information resulting from the narrower line widths, this band is fundamentally more sensitive to the value of the difference potential as discussed elsewhere.[22] The spectra in Figure 4 show that the positions and spacings of the doubled sub-bands in this b-type infrared spectrum change dramatically for modest changes in the value of ρ. Conversely, the simulated spectra also demonstrate that a complete analysis and understanding, even of just the gross features of this band, requires explicit consideration of the partial quenching of OH electronic orbital angular momentum.

As a consequence of the extremely high resolution and lack of predissociation broadening in the microwave, the rotational spectrum of the OH−water complex has the potential to provide an exquisitely detailed picture of this molecule. On the other hand, it will likely be necessary to account for additional interactions, such as magnetic hyperfine interactions and λ-doubling, to fully treat the spectrum to experimental precision. Nevertheless, the rotational transition frequencies for OH−water are clearly affected by the difference potential, and the transition frequencies will not be at simple multiples, neither odd nor even, of the effective rotational constant, $(B + C)/2$, for the intermediate values of ρ predicted for the complex.

Although the OH−water complex is predicted to have a difference potential ($\rho = -110$ to -190 cm^{-1}) similar to that of OH−acetylene ($\rho = -148.1$ cm^{-1} from ref 23), the jet-cooled spectra of the two molecules will have qualitative differences. This occurs as a consequence of the large value of $\sim$13 cm^{-1} for the A rotational constant in OH−water compared to a value of 1.217 cm^{-1} for OH−acetylene.[23] The resulting large separation between rotational energy level manifolds in OH−water leads to a much smaller value of the partition function at the low rotational temperatures appropriate for a supersonic expansion. As a result, only the lowest manifold of each spin symmetry will have population and the spectra have significantly fewer lines. As noted in a previous section, the a-type OH stretch fundamental band is predicted to suffer less inhomogeneous broadening in OH−water than was observed for OH−acetylene,[16] which may reveal the effects of the difference potential more clearly. In the b-type water asymmetric stretching fundamental, the large A constant leads to both fewer sub-bands and a greater separation between sub-band origins. Consequently, the band will be composed of just a few isolated sub-bands spread over many tens of cm^{-1}, whereas the analogous band in OH−acetylene had several sub-bands overlapped in a smaller wavenumber region.[23]

Despite these differences in band contours, the orbital angular momenta in OH−water and OH−acetylene are partially quenched to a similar extent as expected from the similar values for ρ. For the levels contributing to the spectra in Figures 3−5, the OH−water complex has approximately 80−85% A′ character and 15−20% A″.[39] At this level of mixing, approximately 2/3 of the orbital angular momentum remains unquenched as measured by the expectation value of the effective spin−orbit operator, $l_z s_z$.

This degree of orbital angular momentum quenching is significantly less than has been observed for the structurally similar molecules $CaNH_2$ [40,41] and Ca^+-H_2O,[42] in their $\tilde{A}^2B_2$ and $\tilde{B}^2B_1$ excited states. These two states are analogous to the A″ and A′ states, respectively, of OH−water, although the energy ordering is different in the calcium complexes. In these complexes, the magnitude of the difference potential is larger and that of the appropriate spin−orbit constant is smaller (422 and 66 cm^{-1}, respectively for $CaNH_2$ [40] and 1811 and 70−80 cm^{-1}, respectively for Ca^+-H_2O[42]) than is the case for OH−water. The efficiency of quenching increases with the ratio of difference potential to spin−orbit constant, and less than 15% of the orbital angular momentum remains unquenched in the calcium complexes. Each electronic state ($\tilde{A}^2B_2$ and $\tilde{B}^2B_1$) in the calcium complexes is approximately 99% pure with 1% or less of the other state. Consequently, the spectra of the $CaNH_2$ complex have been successfully analyzed by the application of perturbation theory to a zero-order treatment that begins with the completely quenched limit and incorporates the effects of electronic state mixing into the spin-rotation interaction.[40,41] Interestingly, the first analysis of the bands involving these states in $CaNH_2$ used an effective Hamiltonian developed by analogy to the Renner−Teller interaction of triatomic molecules in $^2\Pi$ electronic states and started from the fully unquenched limit,[43] which is similar in spirit to the model used here for OH−water and earlier work on OH−acetylene. This original approach was also used for Ca^+-H_2O,[42] for which the orbital angular momentum is more fully quenched than it is for $CaNH_2$.

V. Conclusions

A model has been developed to treat the rotational energy levels of the OH−water complex with effective C_{2v} symmetry that explicitly accounts for the difference potential, ρ, which is responsible for quenching of the OH orbital angular momentum, and the spin−orbit interaction of the OH monomer. The model is used to generate a correlation diagram (Figure 2) that shows the evolution of the rotational energy levels from P, ω manifolds at small ρ to K_a stacks at large ρ. These changes in the rotational energy level structure are also manifested in the microwave and

infrared spectra of the OH−water complex, where the rotational band structure is shown to be quite sensitive to the magnitude of ρ.

At the ab initio values of ρ, −110 and −190 cm^{-1},[9,21,24,31] the electronic orbital angular momentum as well as the magnetic field that couples the electron spin to the *a* inertial axis will be partially quenched, resulting in OH−water spectra that have a noticeably different appearance than those for the well-known limiting cases of fully quenched or completely unquenched orbital angular momentum. The a-type OH radical stretching band will show complicated P and R branch features as they switch from *odd* to *even* multiples of $(B + C)/2$ with respect to the central Q branch. The b-type water asymmetric stretching band will be even more dramatically affected at these values of ρ, with portions of the sub-bands (primarily Q branches) splitting and shifting as they evolve between the limiting cases of $\Delta(P - \omega) = \pm 1$ (small ρ) and $\Delta K_a = \pm 1$ (large ρ) sub-band structures. The microwave spectrum of the OH−water complex will resemble the a-type band, with R-branch transition frequencies at neither the odd nor even multiples of $(B + C)/2$ characteristic of the small and large ρ limiting cases, respectively. With its high resolution and lack of predissociation broadening, the pure rotational spectrum should clearly show the effects of parity splitting for the $P = 1/2$, $\omega = +3/2$ levels as they evolve into the $K_a = 0$ manifold. Experiments are currently underway to search for the microwave and infrared spectra of the OH−water complex in the gas phase.

Acknowledgment. M.D.M. thanks the H. Axel Schupf '57 Fund for Intellectual Life for supporting his stay at the University of Pennsylvania. M.I.L. acknowledges support from the Office of Basic Energy Sciences of the Department of Energy. The authors also thank Eunice X. J. Li for her help in preparing Figure 1.

Note Added in Proof

After submission of this paper, the OH−water complex has been detected in the gas phase by two groups using FTMW spectroscopy (see refs 44 and 45).

References and Notes

(1) Wayne, R. P. *Chemistry of Atmospheres. An Introduction to the Chemistry of the Atmospheres of Earth, the Planets, and Their Satellites*; Oxford University Press: New York, 1991.

(2) Aloisio, S.; Francisco, J. S. *Acc. Chem. Res.* **2000**, *33*, 825.

(3) Hanson, D. R.; Burkholder, J. B.; Howard, C. J.; Ravishankara, A. R. *J. Phys. Chem.* **1992**, *96*, 4979.

(4) Knipping, E. M.; Lakin, M. J.; Foster, K. L.; Jungwirth, P.; Tobias, D. J.; Gerber, R. B.; Dabdub, D.; Finlayson-Pitts, B. J. *Science* **2002**, *288*, 301.

(5) Johnson, R. E.; Quickenden, T. I. *J. Geophys. Res.*, [*Planets*] **1997**, *102*, 10985.

(6) Langford, V. S.; McKinley, A. J.; Quickenden, T. I. *Acc. Chem. Res.* **2000**, *33*, 665.

(7) Jay-Gerin, J. P.; Ferradini, C. *Chem. Phys. Lett.* **2000**, *317*, 388.

(8) Nanayakkara, A. A.; Balint-Kurti, G. G.; Williams, I. H. *J. Phys. Chem.* **1992**, *96*, 3662.

(9) Xie, Y.; Schaefer, H. F., III. *J. Chem. Phys.* **1993**, *98*, 8829.

(10) Kisiel, Z.; Legon, A. C.; Millen, D. J. *Proc. R. Soc. London, Ser. A* **1982**, *381*, 419.

(11) Kim, H. S.; Kim, H. S.; Jang, J. H.; Kim, H. S.; Mhin, B. J.; Xie, Y.; Schaefer, H. F., III. *J. Chem. Phys.* **1991**, *94*, 2057.

(12) Goldman, N.; Fellers, R. S.; Leforestier, C.; Saykally, R. J. *J. Phys. Chem. A* **2001**, *105*, 515.

(13) Goldman, N.; Leforestier, C.; Saykally, R. J. *J. Phys. Chem. A* **2004**, *108*, 787.

(14) Pfeilsticker, K.; Lotter, A.; Peters, C.; Boesch, H. *Science* **2003**, *300*, 2078.

(15) Kjaergaard, H. G.; Robinson, T. W.; Howard, D. L.; Daniel, J. S.; Headrick, J. E.; Vaida, V. *J. Phys. Chem. A* **2003**, *107*, 10680.

(16) Davey, J. B.; Greenslade, M. E.; Marshall, M. D.; Lester, M. I.; Wheeler, M. D. *J. Chem. Phys.* **2004**, *121*, 3009.

(17) Lester, M. I.; Pond, B. V.; Marshall, M. D.; Anderson, D. T.; Harding, L. B.; Wagner, A. F. *Faraday Discuss.* **2001**, *118*, 373.

(18) Note that the symmetry plane in OH−water is perpendicular to that in OH−acetylene which causes a difference in the labeling of the analogous electronic states.

(19) Langford, V. S.; McKinley, A. J.; Quickenden, T. I. *J. Am. Chem. Soc.* **2000**, *122*, 12859.

(20) Engdahl, A.; Karlström, G.; Nelander, B. *J. Chem. Phys.* **2003**, *118*, 7797.

(21) Cooper, P. D.; Kjaergaard, H. G.; Langford, V. S.; McKinley, A. J.; Quickenden, T. I.; Schofield, D. P. *J. Am. Chem. Soc.* **2003**, *125*, 6048.

(22) Marshall, M. D.; Lester, M. I. *J. Chem. Phys.* **2004**, *121*, 3019.

(23) Marshall, M. D.; Davey, J. B.; Greenslade, M. E.; Lester, M. I. *J. Chem. Phys.* **2004**, *121*, 5845.

(24) Schofield, D. P.; Kjaergaard, H. G. *J. Chem. Phys.* **2004**, *120*, 6930.

(25) Bevan, J. W.; Legon, A. C.; Millen, D. J.; Rogers, S. C. *Chem. Commun.* **1975**, 341.

(26) Bevan, J. W.; Kisiel, Z.; Legon, A. C.; Millen, D. J.; Rogers, S. C. *Proc. R. Soc. London, Ser. A* **1980**, *372*, 441.

(27) Cazzoli, G.; Favero, P. G.; Lister, D. G.; Legon, A. C.; Millen, D. J.; Kisiel, Z. *Chem. Phys. Lett.* **1985**, *117*, 543.

(28) Legon, A. C.; Willoughby, L. C. *Chem. Phys. Lett.* **1983**, *95*, 449.

(29) Harmony, M. D.; Laurie, V. W.; Kuczkowski, R. L.; Schwendeman, R. H.; Ramsay, D. A.; Lovas, F. J.; Lafferty, W. J.; Maki, A. G. *J. Phys. Chem. Ref. Data* **1979**, *8*, 629.

(30) Huber, K. P.; Herzberg, G. *Molecular Spectra and Molecular Structure, vol. 4, Constants of Diatomic Molecules;* Van Nostrand: New York, 1979.

(31) Wang, B. S.; Hou, H.; Gu, Y. S. *Chem. Phys. Lett.* **1999**, *303*, 96.

(32) Huang, Z. S.; Miller, R. E. *J. Chem. Phys.* **1989**, *91*, 6613.

(33) Huisken, F.; Kaloudis, M.; Kulcke, A. *J. Chem. Phys.* **1996**, *104*, 17.

(34) Benedict, W. S.; Gailar, N.; Plyler, E. K. *J. Chem. Phys.* **1956**, *24*, 1139.

(35) Nielsen, H. H. *Phys. Rev.* **1942**, *62*, 422.

(36) Marshall, M. D. Unpublished work.

(37) Green, W. H., Jr.; Lester, M. I. *J. Chem. Phys.* **1992**, *96*, 2573.

(38) These lines are, in fact, split by the spin-rotation interaction, but the splitting, on the order of several megahertz, is too small to be seen in the figure.

(39) This assumes the ab initio sign for ρ.

(40) Marr, A. J.; Tanimoto, M.; Goodridge, D.; Steimle, T. C. *J. Chem. Phys.* **1995**, *103*, 4466.

(41) Morbi, Z.; Zhao, C. F.; Hepburn, J. W.; Bernath, P. F. *J. Chem. Phys.* **1998**, *108*, 8891.

(42) Scurlock, C. T.; Pullins, S. H.; Reddic, J. E.; Duncan, M. A. *J. Chem. Phys.* **1996**, *104*, 4591.

(43) Whitham, C. J.; Jungen, C. *J. Chem. Phys.* **1990**, *93*, 1001.

(44) Brauer, C. S.; Sedo, G.; Grumstrup, E. M.; Leopold, K. R.; Marshall, M. D.; Leung, H. O. *Chem. Phys. Lett.* **2005**, *401*, 420.

(45) Ohsima, Y.; Sato, K.; Sumiyoshi, Y.; Endo, Y. *J. Am. Chem. Soc.* **2005**, *127*, 1108.